

## A Steady-State Modeling Method for Direct Expansion Air Conditioning Systems

Xiling Gao<sup>1</sup>, Rujie Xia<sup>1</sup>, Xiaodong Zhang<sup>2</sup>, Libin Shang<sup>1\*</sup>, Meiqin Xiangli<sup>1</sup>

<sup>1</sup> Jiangsu Vocational Institute of Architectural Technology, XuZhou 221116, China

<sup>2</sup> China Building Technique Group Co., Ltd. Hubei Architectural Design Branch, Wuhan 430070, China

Corresponding Author Email: [10267@jsviat.edu.cn](mailto:10267@jsviat.edu.cn)



<https://doi.org/10.18280/ijht.390632>

### ABSTRACT

**Received:** 17 August 2021

**Accepted:** 24 October 2021

#### Keywords:

*Direct-Expansion Air-Conditioning (DX-AC) system, BP training algorithm, artificial neural network (ANN), steady-state model, bilinear interpolation*

To figure out the operating features of Direct-Expansion Air-Conditioning (DX-AC) system, this paper employed the BP training algorithm and built a two-in/two-out steady-state model based on artificial neural network (ANN) and connect the DX-AC system's Totally output Cooling Capacity (TCC) and Sensible Heat Ratio (SHR) under different combinations of rotational velocities of compressor and blower; then, the paper verified the proposed model by comparing the prediction results of the proposed model with experimental data, and the numerical analysis of the steady-state model and bilinear interpolation indicated that the ANN-based model proposed in the paper showed a high prediction accuracy and can well exhibit its operating performance.

## 1. INTRODUCTION

Air conditioners have been widely used in residential buildings as a necessary equipment that provides a comfortable living environment for people, and the Direct Expansion Air Conditioning (DX-AC) systems, namely the direct evaporation (refrigeration) systems, are one of the most commonly-used air conditioning system types. In a DX-AC system, the evaporator cools and dehumidifies the air directly as a cooling coil. Compared with cold-water central air-conditioning systems [1], DX-AC systems have now been more extensively used in residential buildings due to its many advantages [2] such as simple structure, flexible installation, low maintenance cost, and high energy efficiency. A correct understanding of the steady-state operating features of the variable-velocity DX-AC system is a prerequisite for designing an effective indoor temperature-humidity synchronous control strategy [3], however, such research data is insufficient. The operating features of a DX-AC system include the system TCC and SHR under different compressor-blower velocity combinations.

Previous scholars have developed a few related mathematical models, for instance, Joe J developed a dynamic mathematical model for water-cooled DX-AC systems [4]; Chen constructed a steady-state model to study the operating characteristics of air cooling and coils, and conducted experiments to verify the model [5]. However, the modeling process of these physics-based models is quite complicated, so multiple attempts might be required to get accurate values. ANN is a popular data-driven modeling method that can model complex and nonlinear systems.

To fill in the research gap mentioned above, this paper applied the neural network-based modeling method to the DX-AC systems, and built a two-in/two-out steady-state model based on ANN for the said problem. Then, under the conditions of a fixed inlet air temperature of 24°C and a fixed

relative humidity of 50%, the TCC and SHR were connected under different compressor-blower velocity combinations [6], and the prediction results of the model were compared with test results.

## 2. EXPERIMENTAL CONDITIONS

During the experiment, with the help of a PID (Proportional Integral Derivative) controller, the indoor air dry-bulb temperature of the DX-AC system's cooling coil was controlled at 24°C, and its relative humidity was controlled at 50% [7]; the outdoor air baffle of the DX-AC system was completed closed during the experiment, so no outdoor air had been introduced into the system, and the cooling load of the space was solely provided by the LGUs (Load Generating Units) [8]. Moreover, at a fixed inlet temperature of 35°C, the cooling air flow rate of the condenser was kept at a constant velocity of 3100m<sup>3</sup>/h. Also, with the help of EEV (Electronic Expansion Valve), the degree of superheat of the refrigerant was kept at 6°C by the conventional built-in PID controller.

Considering that the goal of constructing the ANN-based steady-state model [9] is to connect TCC with SHR under different compressor-blower velocity combinations [10], the two velocities were taken as two inputs of the model, and TCC and SHR were regarded as two outputs of the model.

All temperature values during the experiment were measured by a platinum resistance thermometer [11], the report accuracy was  $\pm 0.1^\circ\text{C}$ . The Mass Air Flow (MAF) was measured with a normative nozzle manufactured according to the ANSI/ASHRAE Standard 41.2 (American National Standards Institute/American Society of Heating, Refrigerating and Air-Conditioning Engineers), and the report accuracy was  $\pm 1.2\%$ . When calculating TCC and SHR, the uncertainty of  $U_{TCC}$  and  $U_{SHR}$  was assessed using the classic square root formula:

$$U_{TCC} = \sqrt{\left(\frac{\partial TCC}{\partial m_a} U_{m_a}\right)^2 + \left(\frac{\partial TCC}{\partial T_{db,in}} U_{T_{db,in}}\right)^2 + \left(\frac{\partial TCC}{\partial T_{wb,in}} U_{T_{wb,in}}\right)^2 + \left(\frac{\partial TCC}{\partial T_{db,out}} U_{T_{db,out}}\right)^2 + \left(\frac{\partial TCC}{\partial T_{wb,out}} U_{T_{wb,out}}\right)^2} \quad (1)$$

$$U_{SHR} = \sqrt{\left(\frac{\partial SHR}{\partial T_{db,in}} U_{T_{db,in}}\right)^2 + \left(\frac{\partial SHR}{\partial T_{wb,in}} U_{T_{wb,in}}\right)^2 + \left(\frac{\partial SHR}{\partial T_{db,out}} U_{T_{db,out}}\right)^2 + \left(\frac{\partial SHR}{\partial T_{wb,out}} U_{T_{wb,out}}\right)^2} \quad (2)$$

where,  $T_{db,in}$ ,  $T_{wb,in}$ ,  $T_{db,out}$ ,  $T_{wb,out}$  are respectively the dry-bulb and wet-bulb temperatures of the air entering and leaving the DX-AC system;  $m_a$  represents the MAF;  $U_{TCC}$ ,  $U_{SHR}$ ,  $U_{m_a}$ ,  $U_{T_{db,in}}$ ,  $U_{T_{wb,in}}$ ,  $U_{T_{db,out}}$ ,  $U_{T_{wb,out}}$  respectively represent the uncertainty of TCC, SHR,  $m_a$ ,  $T_{db,in}$ ,  $T_{wb,in}$ ,  $T_{db,out}$ , and  $T_{wb,out}$ . The calculation results showed that the degrees of uncertainty of TCC and SHR caused by measurement errors were 1.85%-3.89% and 1.64%-4.02%, respectively.

The experimental works can be divided into two types: one type was to build steady-state model based on ANN [12]; the other type was to verify the developed model.

### 2.1 Conditions of the first-type experiments

The objective of first-type experiments is to attain test data and connect inputs and outputs of the DX-AC system running under steady-state conditions, and finally get the desired model [13]. To guarantee the maximum model applicability, the input changes should cover the entire operating range of the system during application, therefore, as shown in Table 1, the percentages of maximum compressor velocity ( $P_c$ ) and maximum blower velocity ( $P_F$ ) both changed from 30% to 90% of their respective maximum velocity in steps of 5%, so there're 169 (13×13) velocity combinations in all.

**Table 1.** Velocity combinations in first-type experiments

$P_C$ (%)						
30	35	40	45	50	55	60
65	70	75	80	85	90	
$P_F$ (%)						
30	35	40	45	50	55	60
65	70	75	80	85	90	

The experiments were carried out under the velocity combinations listed in Table 1, and a total of 169 sets of input and output data were generated, which were then used for the training and testing of the proposed model.

### 2.2 Conditions of the second-type experiments

**Table 2.** Velocity combinations in second-type experiments

Nos.	1	2	3	4	5	6	7	8	9	10
$P_C$ (%)	38	43	52	53	62	67	73	78	83	87
$P_F$ (%)	37	82	53	67	83	68	43	52	77	47

The purpose of second-type experiments is to verify the proposed model [14]. The tests were carried out separately from the first-type experiments to independently verify the developed model. The experimental conditions were the same but the combinations of compressor and blower velocities were different, as shown in Table 2, additional tests were conducted under 10 randomly selected compressor-blower velocity combinations, and 10 sets of additional test data of SHR and TCC were obtained. As far as we know, the output

TCC and SHR data of the 10 sets hadn't been used to train or test the ANN.

### 3. THE STEADY-STATE MODEL TRAINING ALGORITHM BASED ON NEURAL NETWORK

The selected NN structure is a multi-layered and feed-forward [15], which is the most commonly-used type in engineering applications. Multi-layer feed-forward neural networks are constructed by sorting neurons hierarchically [16], so that each neuron only takes the output of previous-layer neurons or the external input as its input, in other words, the input signal propagates forward layer by layer in the network [17].

A feed-forward NN with multiple layers generally has three significant features: 1) The model of each neuron in it contains a nonlinear activation function whose nonlinearity is smooth (namely the curve is differentiable everywhere); 2) The network has one or multiple layers of hidden neurons, but are neither part of the inputs nor part of the outputs of the ANN; 3) The network shows high connectivity [18], which is decided by the weight of the ANN. For a feed-forward neural network with multiple layers, it can gain its computing power by integrating these features with its capability to learn from training experience. Figure 1 shows an ordinary multi-layer feed-forward neural network, where  $i$  ( $1 \leq i \leq I$ ) represents the number of layers,  $j$  represents the number of neurons in each layer,  $x$  represents inputting into the neuron,  $y$  represents outputting from the neuron,  $W$  represents the weight of the neural network. Therefore,  $(i, j)$  represents the  $j$ -th neuron in the  $i$ -th network layer, and  $j_i$  represents the total number of neurons in the  $i$ -th layer.

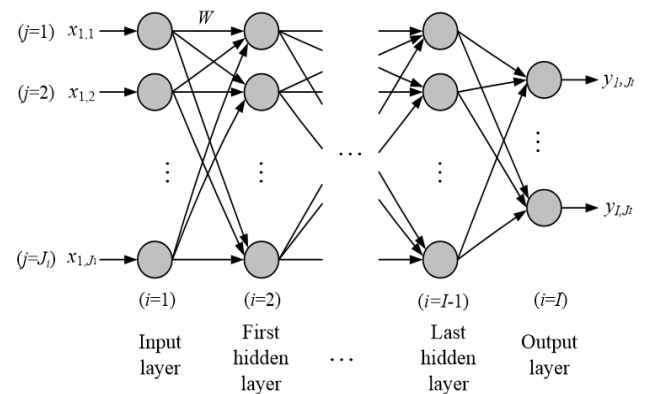


**Figure 1.** Structure of a multi-layer feed-forward neural network

The training algorithm used in the study is the feed-forward back-propagation (BP) algorithm [19]. Each time a set of training data is used to adjust the weights and biases is called a run. A training cycle consists of plentiful enough data to continuously obtain weights and biases from all training data

[20]. Then, the calculation is carried out repeatedly for several cycles, and the relative error (RE) of the  $j$ -th neuron in the output layer of the  $n$ -th dataset in the last cycle can be determined by the following formula:

$$RE_j^n = \frac{|O_{i,j}^n - y_{i,j}^n|}{O_{i,j}^n} \quad (3)$$

During the test, two indicators  $R$  and  $\sigma$  were adopted to assess the performance of different ANN configurations and the sensitivity of the REs and standard deviations of all test data [21], as shown in the following formulas:

$$R = \frac{1}{J_1} \sum_{j=1}^{J_1} R_j = \frac{1}{J_1} \frac{1}{N} \sum_{j=1}^{J_1} \sum_{n=1}^N R_j^n = \frac{1}{J_1} \frac{1}{N} \sum_{j=1}^{J_1} \sum_{n=1}^N \frac{y_{i,j}^n}{O_{i,j}^n} \quad (4)$$

$$\sigma = \frac{1}{J_1} \sum_{j=1}^{J_1} \sigma_j = \frac{1}{J_1} \sum_{j=1}^{J_1} \sqrt{\frac{1}{N} \sum_{n=1}^N (R_j - R_j^n)^2} \quad (5)$$

where,  $N$  is the total number of datasets adopted in training or testing,  $O_{i,j}^n$  is the target output,  $y_{i,j}^n$  is the output of ANN corresponding to  $O_{i,j}$  during the test,  $R$  represents the average prediction accuracy, and  $\sigma$  represents the prediction dispersion of the ANN [22].

#### 4. DEVELOPMENT OF THE STEADY-STATE MODEL BASED ON ANN

During the research, 144 datasets (85% of the total 169 datasets) were randomly chosen for training, and the rest 25 datasets (15% of the total 169 datasets) were chosen for testing. In order to choose ANN with appropriate configurations when modeling the DX-AC system, 4 evaluation indicators listed in Table 3 were adopted to evaluate many different ANN configurations. One thing needs to be pointed out is that, the first 2 indicators were attained from the training process, and the other 2 were attained from the testing process. The first 2 indicators, average relative error (ARE) and maximum relative error (MRE), were evaluated in the following ways:

$$ARE = \frac{1}{J_1} \frac{1}{N} \sum_{j=1}^{J_1} \sum_{n=1}^N RE_j^n = \frac{1}{J_1} \frac{1}{N} \sum_{j=1}^{J_1} \sum_{n=1}^N \frac{|y_{i,j}^n - O_{i,j}^n|}{y_{i,j}^n} \quad (6)$$

$$MRE = \text{Max}(RE_j^n) \quad (7)$$

**Table 3.** Accuracy evaluation indicators of different ANN configurations

Indicator	Definition
ARE	The average relative error of the last cycle during the test
MRE	The maximum relative error of the last cycle during the test
R	The average ratio of test data to corresponding ANN output
$\sigma$	The standard deviation between test data and corresponding ANN output

The setting of ANN configurations would determine the

precision of ANN in training and testing. Finally, the 2-6-6-2 structure given in Figure 2 was chosen as the configuration, since the values of  $ARE$  and  $MRE$  were at their respective lowest of 0.026 and 0.0046, indicating that the data accuracy during model training was relatively high; the  $\sigma$  value was at its lowest 0.0052 and the  $R$  value was close to the ideal expectation of 0.9985, indicating that the developed ANN model had a high average accuracy and a low dispersion.

Figures 3 and 4 show the experimental data used to develop the proposed model. The 144 datasets adopted for training are shown as grid points on two spatial surfaces, and the rest 25 datasets are shown as crosses. Using the established neural network model, the calculation results and experimental results of TCC and SHR of different  $P_c$  and  $P_f$  combinations were compared. For the model developed based on 2-6-6-2 ANN, Figure 5 gives all data in the test. As shown in the figure, most relative errors of the calculation were lower than 0.015, only four values were greater than 0.015, indicating that the proposed model showed high prediction accuracy during the operation in the experiments.

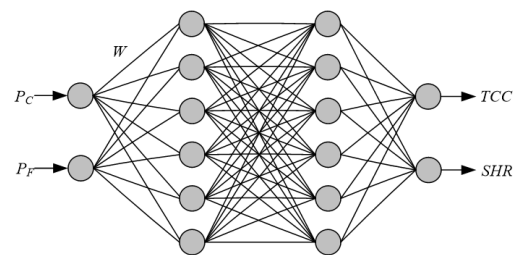


**Figure 2.** The selected 2-6-6-2 neural network structure

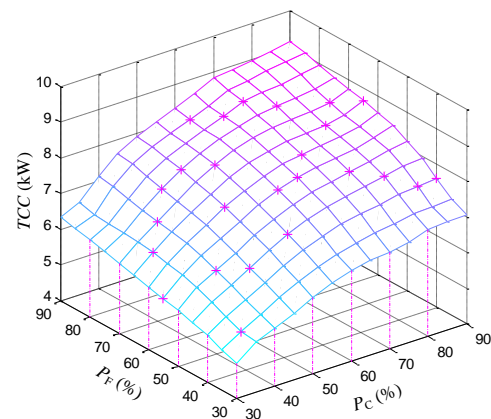


**Figure 3.** The TCC data used for training and testing

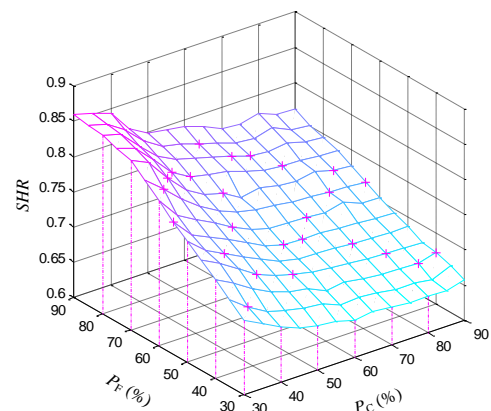


**Figure 4.** The SHR data used for training and testing

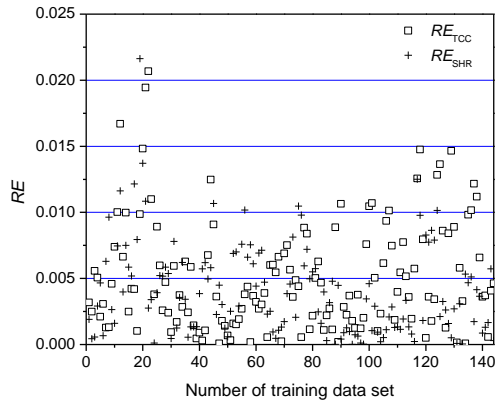


**Figure 5.** Distribution of RE of the proposed 2-6-6-2 ANN model

## 5. VERIFICATION OF THE PROPOSED MODEL

With the help of the constructed ANN model, the SHR and TCC values can be forecast. In order to verify the prediction accuracy of the model, 10 sets of additional test data were attained, as shown in Table 4. Under the 10 velocity combinations, the prediction results of the model and the corresponding experimental results were compared to verify the prediction performance of the model, as shown in Table 4, all relative errors of the calculations were lower than 4%, and most of them were less than 1%.

**Table 4.** The relative errors between prediction results and experimental results

Nos.	$P_C$ (%)	$P_F$ (%)	$RE_{TCC}$ (%)	$RE_{SHR}$ (%)
1	38	37	0.3141	0.7913
2	43	82	0.3686	1.6348
3	52	53	0.6863	0.2218
4	53	67	1.0145	0.0821
5	62	83	1.6506	1.0782
6	67	68	0.4714	0.3063
7	73	43	0.6205	0.9825
8	78	52	0.7146	0.1237
9	83	77	3.6206	1.6342
10	87	47	0.4266	0.6757

Using this physics-based steady-state model [23], the prediction accuracy of the relative errors of SHR was around 6%, much higher than errors listed in Table 4, showing that the developed model had a high prediction accuracy. In addition, another advantage of the model is that it is simpler than the physics-based model which focuses on basic physical processes, the latter often involves many calculation equations [24], and it has to make many assumptions during the development process.

Moreover, bilinear interpolation can extend linear interpolation to two dimensions [25]. By applying it, we can use experimental data to evaluate TCC and SHR values of the 10 prediction points specified in Table 4, and calculate the relative errors between the prediction results and the experimental results [26]. Figure 6 gives a comparison of the relative errors of TCC, and Figure 7 gives a comparison of the relative errors of SHR between the ANN-based model and the bilinear interpolation. The comparison results showed that, compared with other prediction methods, the accuracy of the model developed based on ANN was acceptable, therefore the

developed model could be used as a good alternative for simulating DX-AC systems [27].



**Figure 6.** RE of TCC between proposed model and bilinear interpolation

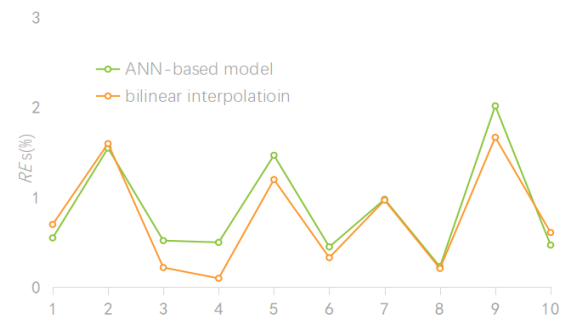


**Figure 7.** RE of SHR between proposed model and bilinear interpolation

## 6. CONCLUSION

Applying BP training algorithm, this paper connected steady-state TCC and SHR of the DX-AC system under different compressor and blower velocity combinations, and developed a two-in two-out steady-state neural network model. A total of 144 datasets were used for training and 25 datasets were used for testing. By comparing the measurement results of TCC and SHR of 10 additional combinations of compressor and blower velocities with the prediction results of the steady-state model developed based on ANN, the proposed model was verified by experimental results. When the proposed model was applied in prediction, all relative errors were less than 4%, and most of them were less than 1%, indicating that the proposed model had a high prediction accuracy.

The experiments on the steady-state model of DX-AC system with multiple input and output variables based on neural network indicated that the applied neural network can well represent its operating performance. The ANN-based steady-state model is helpful for researchers to figure out the operating performance of DX-AC systems, so that appropriate controllers could be developed for DX-AC systems to realize the control of indoor air temperature and humidity at the same time.

## ACKNOWLEDGMENT

This paper is supported by the science and technology

project of Jiangsu Provincial Department of housing and urban rural development (Grant No.: 2019ZD001149) and the scientific research project of Jiangsu Vocational Institute of Architectural Technology in 2021 (Grant No.: JYA320-11).

## REFERENCES

- [1] Al-Okbi, A., Vankov, Y., Kadhim, H. (2021). Improving performance of direct expansion air conditioning systems while reducing electricity consumption through using hybrid energy. *E3S Web of Conferences*, 289: 01014. <https://doi.org/10.1051/E3SCONF/202128901014>
- [2] Gao, X., Shang, L., Xia, R., Zhang, X., Yao, W. (2021). Influence of air supply height on sleep comfort through computational fluid dynamics simulation. *International Journal of Heat and Technology*, 39(4): 1173-1179. <https://doi.org/10.18280/IJHT.390415>
- [3] De Masi, R.F., Gigante, A., Festa, V., Ruggiero, S., Vanoli, G.P. (2021). Effect of HVAC's management on indoor thermo-hygrometric comfort and energy balance: In situ assessments on a real nZEB. *Energies*, 14(21): 7187. <https://doi.org/10.3390/EN14217187>
- [4] Joe, J., Im, P., Dong, J. (2020). Empirical modeling of direct expansion (Dx) cooling system for multiple research use cases. *Sustainability (Switzerland)*, 12(20): 1-17. <https://doi.org/10.3390/SU12208738>
- [5] Chen, W., Chan, M. yin, Weng, W., Yan, H., Deng, S. (2018). Development of a steady-state physical-based mathematical model for a direct expansion based enhanced dehumidification air conditioning system. *International Journal of Refrigeration*, 91: 55-68. <https://doi.org/10.1016/J.IJREFRIG.2018.04.028>
- [6] Afram, A., Janabi-Sharifi, F., Fung, A.S., Raahemifar, K. (2017). Artificial neural network (ANN) based model predictive control (MPC) and optimization of HVAC systems: A state of the art review and case study of a residential HVAC system: A state of the art review and case study of a residential HVAC system. *Energy and Buildings*, 141: 96-113. <https://doi.org/10.1016/J.ENBUILD.2017.02.012>
- [7] Abdullah, A.N., Ali, M.H. (2020). Direct torque control of IM using PID controller. *International Journal of Electrical and Computer Engineering*, 10(1): 617-625. <https://doi.org/10.11591/IJECE.V10I1.PP617-625>
- [8] Aboelhassan, A., Abdelgelil, M., Zakzouk, E.E., Galea, M. (2020). Design and implementation of model predictive control based PID controller for industrial applications. *Energies*, 13(24): 6594. <https://doi.org/10.3390/EN13246594>
- [9] Nakabi, T.A., Toivanen, P. (2019). An ANN-based model for learning individual customer behavior in response to electricity prices. *Sustainable Energy, Grids and Networks*, 18: 100212. <https://doi.org/10.1016/J.SEGAN.2019.100212>
- [10] Khan, M.M.H., Muhammad, N.S., El-Shafie, A. (2018). Wavelet-ANN versus ANN-based model for hydrometeorological drought forecasting. *Water*, 10(8): 998. <https://doi.org/10.3390/W10080998>
- [11] Campos, J.A., Pedrollo, O.C. (2021). A regional ANN-based model to estimate suspended sediment concentrations in ungauged heterogeneous basins. *Hydrological Sciences Journal*, 66(7): 1222-1232. <https://doi.org/10.1080/02626667.2021.1918695>
- [12] Vakiloroyaya, V., Samali, B., Pishghadam, K. (2014). A comparative study on the effect of different strategies for energy saving of air-cooled vapor compression air conditioning systems. *Energy and Buildings*, 74: 163-172. <https://doi.org/10.1016/J.ENBUILD.2014.01.042>
- [13] Yilmaz, C., Koyuncu, I. (2021). Thermo-economic modeling and artificial neural network optimization of Afyon geothermal power plant. *Renewable Energy*, 163: 1166-1181. <https://doi.org/10.1016/J.RENENE.2020.09.024>
- [14] Ullah, S., Tanyu, B.F., Zainab, B. (2020). Development of an artificial neural network (ANN)-based model to predict permanent deformation of base course containing reclaimed asphalt pavement (RAP). *Road Materials and Pavement Design*, pp. 1-19. <https://doi.org/10.1080/14680629.2020.1773304>
- [15] Alahassa, N.K.A. (2021). State-of-the-art multivariate regression with a general Nk hidden multi-layer feed forward neural network model. *ICAICST 2021 - 2021 International Conference on Artificial Intelligence and Computer Science Technology*, pp. 31-36. <https://doi.org/10.1109/ICAICST53116.2021.9497838>
- [16] Baek, S., Imakura, A., Sakurai, T., Kataoka, I. (2021). Accelerating the backpropagation algorithm by using NMF-Based method on deep neural networks. In *Pacific Rim Knowledge Acquisition Workshop*, pp. 1-13. [https://doi.org/10.1007/978-3-030-69886-7\\_1](https://doi.org/10.1007/978-3-030-69886-7_1)
- [17] Arslan, Ö., Engin, E.Z. (2019). Noise robust voice activity detection based on multi-layer feed-forward neural network. *Electrica*, 19(2): 91-100. <https://doi.org/10.26650/ELECTRICA.2019.18042>
- [18] Al Tobi, M., Bevan, G., Wallace, P., Harrison, D., Okedu, K.E. (2021). Faults diagnosis of a centrifugal pump using multilayer perceptron genetic algorithm back propagation and support vector machine with discrete wavelet transform-based feature extraction. *Computational Intelligence*, 37(1): 21-46. <https://doi.org/10.1111/COIN.12390>
- [19] Issac, T., Silas, S., Rajsingh, E.B. (2021). System modeling and simulation of an outdoor illumination system using a multi-layer feed-forward neural network. *Advances in Intelligent Systems and Computing*, 1167: 495-507. [https://doi.org/10.1007/978-981-15-5285-4\\_49](https://doi.org/10.1007/978-981-15-5285-4_49)
- [20] Kumar, A., Sinwar, D., Saini, M. (2021). Study of several key parameters responsible for COVID-19 outbreak using multiple regression analysis and multi-layer feed forward neural network. *Journal of Interdisciplinary Mathematics*, 24(1): 53-75. <https://doi.org/10.1080/09720502.2020.1833443>
- [21] García-Ródenas, R., Linares, L.J., López-Gómez, J.A. (2021). Memetic algorithms for training feedforward neural networks: an approach based on gravitational search algorithm. *Neural Computing and Applications*, 33(7): 2561-2588. <https://doi.org/10.1007/S00521-020-05131-Y>
- [22] Moradkhani, E., Mola, M. (2021). Intelligent modeling of cement plant mill unit using artificial neural networks and real data. In *2021 International Siberian Conference on Control and Communications (SIBCON)*, pp. 1-6. <https://doi.org/10.1109/SIBCON50419.2021.9438907>
- [23] Li, D., Koopialipoor, M., Armaghani, D.J. (2021). A combination of fuzzy Delphi method and ANN-based models to investigate factors of flyrock induced by mine blasting. *Natural Resources Research*, 30(2): 1905-1924.

- <https://doi.org/10.1007/S11053-020-09794-1>
- [24] Benner, P., Gugercin, S., Werner, S.W. (2021). Structure-preserving interpolation of bilinear control systems. *Advances in Computational Mathematics*, 47(3): 1-38. <https://doi.org/10.1007/S10444-021-09863-W>
- [25] Kim, K.H., Shim, P.S., Shin, S. (2019). An alternative bilinear interpolation method between spherical grids. *Atmosphere*, 10(3): 123. <https://doi.org/10.3390/ATMOS10030123>
- [26] Mastyló, M. (2013). Bilinear interpolation theorems and applications. *Journal of Functional Analysis*, 265(2): 185-207. <https://doi.org/10.1016/J.JFA.2013.05.001>
- [27] Tsimpoukis, D., Syngounas, E., Petsanas, D., Mitsopoulos, G., Anagnostatos, S., Bellos, E. (2021). Energy and environmental investigation of R744 all-in-one configurations for refrigeration and heating/air conditioning needs of a supermarket. *Journal of Cleaner Production*, 279: 23234. <https://doi.org/10.1016/J.JCLEPRO.2020.123234>